

RICE UNIVERSITY

**Controls on magma supply from depth at Kīlauea
Volcano, Hawai‘i**

by

Austin P. Blaser

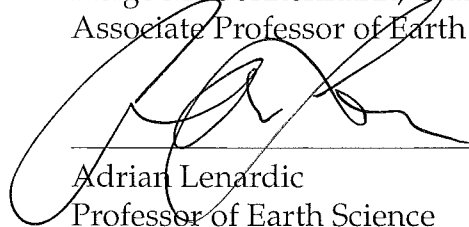
A THESIS SUBMITTED
IN PARTIAL FULFILLMENT OF THE
REQUIREMENTS FOR THE DEGREE

Master of Science

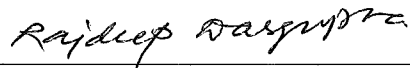
APPROVED, THESIS COMMITTEE:



Helge M. Gonnermann, Chair
Associate Professor of Earth Science



Adrian Lenardic
Professor of Earth Science



Rajdeep Dasgupta
Professor of Earth Science

Houston, Texas

April, 2016

ABSTRACT

Controls on magma supply from depth at Kīlauea Volcano, Hawai‘i

by

Austin P. Blaser

Volcanic activity at Kīlauea volcano, Hawai‘i, Earth’s most active volcano, is thought to be the consequence of more or less continuous flow of magma from the asthenospheric melting region through an essentially open lithospheric pathway to a magma storage system located at a depth of a few kilometers beneath the volcano’s summit. The rate of magma supply from depth to the Kīlauea’s summit is, however, not constant through time. For example, during the current Pu‘u Ō‘ō-Kupaianaha eruption (1983-present), a surge in supply occurred between 2003-2007. This surge was accompanied by summit inflation, increased CO₂ and SO₂ emissions, and ultimately led to dike intrusion, explosive activity, as well as increased rates in the volume of erupted magma. It has been suggested that a surge in magma supply may be the result of an increase in volatile content of the melt or, alternatively, a change in the magma pressure conditions at depth, perhaps due to some intermittent increase in permeability of the melting region. I use a numerical model of two-phase (gas-melt) magma flow through an idealized lithospheric magma pathway to explore the role of volatile content, pathway geometry, and magma pressure on the rate of magma supply to Kīlauea’s summit magma storage system. My results suggest that volatiles have a limited role in increasing supply rate. Instead, changes in magma pressure at depth, of the order of 10⁵ Pa, suf-

face to produce two-fold changes in magma supply rate. Moreover, because of the coupling between magma pressure within the lithospheric plumbing system and resultant deformation of the surrounding rock, it is feasible that magma pressure at depth is dynamically decoupled from changes in magma pressure of the summit storage system, caused by short- or long-term changes in eruptive or intrusive activity. In other words, whereas magma supply and overall activity at Kīlauea seem to be controlled from the bottom up, the details of Kīlauea's volcanic activity are modulated by shallow processes that seem unlikely to affect the deeper magma supply and transport system.

ACKNOWLEDGEMENTS

I would first like to acknowledge Dr. Helge Gonnermann for his critical role as my advisor in shaping the development of my research, as well as influencing my time as graduate student and developing scientist. I appreciate many valuable lessons including thinking critically, and how to approach solving a complex problem. I thank him for his support of me in exploring a range of careers and offering professional advice.

I thank my family, in particular my parents Eric and Liz, for supporting me over these years and for always emphasizing the value of an education.

I would also like to thank my fellow Rice graduate students and post-doctoral fellows, in particular Pranabendu Moitra, Chinh Nguyen, Sahand Hajirmirza, and Alana Semple for many helpful scientific discussions, plenty of laughs, and unrelenting support during my time at Rice. I also thank Thomas Giachetti, Chiara Montagna, and Amalia Bonanno. I offer special thanks to Laura Carter and Lacey Pyle for great support as well.

Finally, I thank the Earth Science Department staff, and in particular Mary Ann Lebar, Soookie Sanchez, and Bonnie Hoffman.

Contents

Abstract	ii
Acknowledgements	iv
List of Illustrations	vii
List of Tables	xi
1 Controls on magma supply from depth at Kīlauea Volcano, Hawai‘i	1
1.1 Introduction	1
1.1.1 Objective	1
1.2 Overview of Kīlauea’s magmatic system	2
1.2.1 Kīlauea’s plumbing system	2
1.2.2 Estimated magma supply rates	5
1.2.3 The 2003-07 magma supply ‘surge’	5
1.3 Conceptual model	7
1.3.1 Observational constraints on magma supply	7
1.3.2 Model rationale	8
1.3.3 Essence of the model	9
1.4 Numerical model	10
1.4.1 Governing equations	10
1.4.2 Initial values	13
1.4.3 Outflow and Storage	14
1.4.4 Volatiles	14
1.4.5 Lithostatic stress	15

1.5	Results	16
1.5.1	Non-dimensional analysis	16
1.5.2	Dimensional model, with application to Kīlauea	17
1.6	Conclusion	19
2	Appendix	29
2.1	Olivine crystallization	29
2.2	Calculating the spatial gradient in mixture density	30
2.3	CO ₂ -H ₂ O solubility and gas density	31
2.4	Melt density and compressibility	31
2.5	Non-dimensional analysis	32
2.6	Sensitivity to N_b	35
	Bibliography	39

Illustrations

- 1.1 Shaded-relief map showing the southern half of the island of Hawai‘i along with notable features of the volcanic system, including the East Rift Zone (ERZ). Inset map was generated using GMT Plotting Tools. 21
- 1.2 Conceptual model of the magmatic plumbing system beneath Hawai‘i, including Kīlauea. The letters **M**, **K**, **P**, and **L**, represent Mauna Loa, Kīlauea, Pu‘u ‘Ō‘ō, and Loih‘i, respectively. 21
- 1.3 Magma supply rates from *Wright and Klein* (2014). These rates are estimated by the eruptive and intruded volumes over specific time scales. Supply increased from 1960-1995, but not as dramatically as the 2003-2007 magma surge. 22
- 1.4 Figure showing the measured CO₂ emissions at Kīlauea’s summit (*Poland et al.*, 2012). Before the end of 2003, CO₂ emissions remained relatively steady at approximately 8,000 tonnes per day. By 2005, however, emissions increased to nearly 20-30 kilotonnes per day. Emissions began to fall and by 2011 had returned to their pre-surge levels. Black trend lines represent a least squares best fit through the data. 22

- 1.5 Conceptual model. Melt generated in the asthenospheric melt zone begins to ascend within a dike-shaped conduit, with pressure, P_b . Vapor-filled bubbles form once the ascending melt reaches a pressure where CO_2 saturates. As the magma continues to rise, more CO_2 exsolves and the bubbles grow, becoming more buoyant and rising faster than the host melt. A drift-flux formulation accounts for the differential velocity between the vapor and melt. Finally, magma exits the lithospheric pathway with pressure P_t and flow rate Q , where it may interact with summit reservoir(s) or enter the East Rift Zone (ERZ). The aperture of the dike depends on the overpressure in magma and thus is variable with depth. 23
- 1.6 Plot of CO_2 - H_2O solubility (*Dixon, 1997*), bulk magma density (*Lange, 1994*) under static closed-system conditions, and lithostatic density as functions of depth. For the depths considered in this model, CO_2 is the dominant component of the vapor phase. 24
- 1.7 Non-dimensional dike width, $\hat{b} = b/b_t$, as a function of non-dimensional depth, $\hat{z} = z/b_t$, for a range of overpressures in a magma chamber ($\hat{z} = 0$). Shown here is one dike that widens with depth, and several others that narrow with depth. At a unique depth ratio \hat{z} for each set of boundary conditions, dikes no longer change width. 24
- 1.8 Figure displaying the relationship of equilibrium ($d\hat{b}/d\hat{z} = 0$) values of \hat{b} and its corresponding depth ratio, \hat{z} . Interestingly, two distinct regimes exist: dikes that widen with depth and those that narrow with depth. 25
- 1.9 Various parameters of a pre-surge reference case where $Q = 0.18 \text{ km}^3/\text{yr}$ and $\Delta P_t = 5 \text{ MPa}$, and a primary melt containing 0.7 wt% CO_2 and 0.68 wt% H_2O 25

- 1.10 Predicted supply to Kīlauea volcano for a range of overpressures (magma pressure in excess of lithostatic) at the base of the lithosphere (ΔP_b). 26
- 1.11 Dike width verses depth for a range of overpressures (magma pressure in excess of lithostatic) at the summit chamber. Below the Moho, all dikes converge to a similar width, regardless of their overpressure in the summit chamber. This *decoupling* of overpressure near the surface and depth suggests that surface conditions have limited effect on supply rate. 26
- 1.12 Predicted supply to Kīlauea volcano for melts containing a range of CO₂ and H₂O. A factor of 1 indicates a primary melt composition of 0.7 wt% CO₂ and 0.68 wt% H₂O. Blue curve represents melts that only change in CO₂ whereas the red curve represents melts whose variability is in both volatile species. A change in slope between 1.6 and 1.8 marks the transition from melts that saturate in CO₂ at depths shallower than the inferred lithosphere-asthenosphere boundary (50 km depth) and those that exsolve a vapor phase at pressures higher than those found at 50 km depth. 27
- 2.1 Predicted supply rate to Kīlauea for a range of ΔP_b for a range of plausible bubble number densities. There is no significant difference in flow rate for a given ΔP_b for a range of bubble number densities. 36

- 2.2 Plots comparing spatial derivatives of mixture density, $d\rho/dz$, as functions of depth. The closed system defines mixture density based on a gas fraction derived from a closed system degassing path, instead of a drift flux value of ϕ . It implies a complete coupling of the vapor phase to the melt. In contrast, the open system bases its mixture density on a gas fraction calculated from drift flux, allowing for a decoupled vapor phase. The open system is calculated *a posteriori* to evaluate the accuracy of using a closed system approximation (Eq. 2.2). The lower plot indicates the fractional error of the approximation, which exceeds 20 near the top of the lithospheric pathway. Due to this error, future iterations will require an implementation of Equation 2.2 in place of the closed system assumption. 37
- 2.3 Stoke's velocity versus radius of an olivine crystal suspended in a basaltic melt. Since Stoke's velocity depends on the density of the magma, two curves are plotted that represent an upper and lower bound of magma densities used in the model. Over the size range of olivine crystals reported from other melt inclusion studies (*Clague and Denlinger, 1994; Sides et al., 2014*), velocity varies approximately one order of magnitude, but remains at least an order of magnitude lower than the mixture velocity. For reference, the maximum velocity of the gas phase relative to the melt is plotted. 38

Tables

1.1	Table listing variables and descriptions used in the model.	28
2.1	Table reproduced in part from Table 11-2 of <i>Todreas and Kazimi</i> (1989), describing values of n and V_{∞}	36

Chapter 1

Controls on magma supply from depth at Kīlauea Volcano, Hawai‘i

1.1 Introduction

1.1.1 Objective

Kīlauea volcano, Hawai‘i, is the most active volcano on Earth (Figure 1.1). Over the last century, it has had several periods of eruptive activity (e.g., *Klein, 1982; Poland et al., 2014*). The most recent of these, the Pu‘u ‘Ō‘ō-Kupaianaha eruption, began in 1983 and continues to the present (2016).

Persistent gas emissions, in particular CO₂ and SO₂ (*Elias and Sutton, 2007, 2012; Poland et al., 2012*), near continuous eruptive activity over decades, as well as correlation between deep seismicity and volcanic activity suggest an open magma pathway between asthenospheric melt source and the surface (*Wright and Klein, 2014*). This is also consistent with geochemical data that allow mantle-derived compositional variation in erupted lavas to be resolved down to time scales of years (*Pietruszka et al., 2001; Reiners, 2002; Greene et al., 2013*).

Individual eruptive episodes seem largely controlled by processes within the upper few kilometers below the surface, such as magma and/or gas accumulation within shallow storage reservoirs (e.g., *Wilson and Head, 1988; Cervelli and Miklius,*

2003; Poland *et al.*, 2009), changes in the flow capacity of magma pathways (Miklius and Cervelli, 2003), as well as diking events (e.g., Poland *et al.*, 2009; Montgomery-Brown, 2010). But what causes significant changes in eruptive and intrusive activity at Kīlauea over timescales of years?

Suggested mechanisms include time-dependent melt production rates of the mantle source (Pietruszka *et al.*, 2015), as well as variability in the volatile content of the primary mantle-derived melt (Sides *et al.*, 2014). The objective of the work presented herein is to test these hypotheses by assessing the fundamental conditions of lithospheric magma transport at different, but constant, rates of magma supply to Kīlauea volcano, using a numerical model to simulate upward flow of magma.

1.2 Overview of Kīlauea's magmatic system

1.2.1 Kīlauea's plumbing system

The source of Kīlauea's magma is thought to be a region of partial asthenospheric melting within anomalously hot, buoyantly upwelling mantle (e.g., Morgan, 1971; Frey and Rhodes, 1993; DePaolo and Stolper, 1996; Wolfe *et al.*, 2009; Cao *et al.*, 2011; Rychert *et al.*, 2013). Due to the density difference between melt and residual mantle, compaction of the partially molten asthenosphere is thought to result in upward flow of melt toward the lithospheric plumbing systems of the overlying active Hawaiian volcanoes, that is Mauna Loa, Kīlauea and Loih'i (Eaton and Murata, 1960; McKenzie, 1984; Scott and Stevenson, 1984; Tilling and Dvorak, 1993; Maaløe,

1998, 1999) (see Figure 1.2). Although this compaction-driven asthenospheric melt flow has generally been treated as Darcian (*Sleep, 1974; Turcotte and Ahern, 1978; Maaløe and Hansen, 1982; McKenzie, 1984; Scott and Stevenson, 1986; Ribe and Smooke, 1987; Spiegelman and Elliott, 1993*), it is likely that such permeable flow is not only at the grain scale, but also involves flow through veins that may evolve over time due to deformation (*Maaløe, 2003, 2005; Katz et al., 2006; Holtzman et al., 2003; Holtzman and Kohlstedt, 2007*), perhaps resulting in spatiotemporal variations in effective permeability.

Ultimately, the melt must be focused into a lithospheric feeder system (*Eaton and Murata, 1960; Tilling and Dvorak, 1993; Maaløe, 1998, 1999; Wright and Klein, 2006*), which appears to remain open for decades in order to supply magma to Kīlauea's summit during periods of prolonged activity, such as the Pu'u Ō'ō-Kupaianaha eruption (1983 - present).

Kīlauea's summit storage is comprised of several geodetically distinct inflation/deflation regions, thought to represent regions of primary magma storage, that appear to be dynamically interconnected. One such region is located beneath the southern part of Kīlauea caldera, at a depth of approximately 3 km. It is called the *South Caldera Reservoir* and has a volume of 3 to 20 km³ (*Poland et al., 2014; Wright and Klein, 2014*). A smaller deformation source is located at approximately 1-2 km beneath the east margin of Halema'uma'u crater. It has a volume 0.2-1.2 km³ and is called the *Halema'uma'u reservoir*. A third geodetically discernible deformation source and is located at a depth of 2.0-4.9 km near Keanakāko'i Crater.

Over the past decades all magma entering from below into Kīlauea's summit storage system either resides within parts of this storage system for some time or flows laterally into the East Rift Zone (denoted ERZ hereafter). Most of the magma entering the ERZ erupts, and during the past decades the primary locus of eruptive activity has been at the Pu'u 'Ō'ō vent, located in the ERZ approximately 15 km from Kīlauea's summit. Although the ERZ represents an extensional lineament that terminates Kīlauea's south flank, which is sliding seaward along a décollement associated with the interface between ocean floor and Kīlauea's volcanic edifice (*Cayol et al., 2000; Thornber et al., 2003; Wright and Klein, 2008; Montgomery-Brown et al., 2009; Montgomery-Brown, 2010; Montgomery-Brown et al., 2011*), it also is a sub-horizontal magma pathway, thought to have initiated as a dike intruding at the level of magma neutral buoyancy (e.g., *Eaton and Murata, 1960; Zucca et al., 1982; Ryan, 1987; Lister and Kerr, 1991; Head and Wilson, 1992; Walker, 1992; Ryan, 1993; Borgia, 1994; Delaney et al., 1998; Morgan et al., 2003*). The hydraulic connection between Kīlauea's summit and the ERZ is complex, with erupted magmas passing through different parts of the summit magma storage system (*Garcia et al., 1996, 1998, 2000, 2003; Thornber et al., 2003; Marske et al., 2008; Greene et al., 2013*); however, there appears to be a strong connection to the South Caldera Reservoir.

1.2.2 Estimated magma supply rates

The mantle-derived magma supply to Kīlauea's summit magma storage system is thus balanced by magma storage within the summit and rift zones, dike intrusion and magma eruption (*Delaney and McTigue, 1994; Denlinger, 1997; Cayol et al., 2000; Poland et al., 2014; Wright and Klein, 2014*). Magma supply rate estimates for the past century range between approximately 0.02 and 0.4 km³ yr⁻¹ (*Poland et al., 2014; Wright and Klein, 2014*), with approximately 0.18 km³ yr⁻¹ during the two decades prior to 2003 (see Figure 1.3).

1.2.3 The 2003-07 magma supply 'surge'

Major changes in activity at Kīlauea, and variations in the composition of erupted lavas, have been attributed to variations in magma supply. For example, it has been suggested that eruptive activity at Kīlauea's summit may be associated with periods of low supply, whereas sustained rift eruptions are favored when supply rates are high (*Dvorak and Dzurisin, 1993; Wright and Klein, 2014*). A more recent, well-documented episode of change in Kīlauea's magma supply occurred in 2003-2007, referred to as the *2003-07 magma supply surge* (*Poland et al., 2012*). Beginning in mid-2002, nearly two decades of slow deflation of Kīlauea's summit ended as the summit began to inflate. After accelerating in 2005, an inflationary trend continued through most of June 2007, resulting in nearly 0.3 m of vertical uplift. Finally in mid-June 2007, deflation commenced as dikes intruded into the ERZ leading to a fissure eruption and formation of a new long-term eruptive vent about 2 km

down-rift of Pu‘u ‘Ō‘ō (*Poland et al.*, 2008, 2009; *Montgomery-Brown*, 2010; *Poland et al.*, 2012).

In general, inflation at Kīlauea’s summit is thought to be the result of a higher magma supply arriving from depth than is flowing into the ERZ and/or erupting. Likewise, summit deflation occurs when supply from depth is less than the outflow, meaning that there is a net loss of summit-stored magma due to flow into the ERZ. During the 2003-07 surge, eruptive activity along the ERZ showed no change until 2005, when SO₂ emissions at Pu‘u ‘Ō‘ō nearly doubled, presumably indicating an increase in eruption rate (*Elias and Sutton*, 2007) and, hence, increased magma flow from summit to ERZ. Continued inflation of Kīlauea’s summit during 2005-2007 likely indicates that supply continued to outpace magma flow from summit into the ERZ. The resultant stress build-up due to the imbalance between supply and outflow was eventually relieved by the 17-19 June, 2007 dike intrusion between the summit and Pu‘u ‘Ō‘ō and subsequent activity further down-rift, resulting in summit deflation (*Poland et al.*, 2008, 2009; *Montgomery-Brown*, 2010; *Poland et al.*, 2012).

The 2003-07 magma surge was accompanied by an increase in summit CO₂ emissions (see Figure 1.4, *Elias and Sutton*, 2007; *Hager et al.*, 2008; *Poland et al.*, 2012; *Elias and Sutton*, 2012), interpreted to reflect an increase in magma supply. The CO₂ content of Kīlauea’s parental melts is estimated to be approximately 0.7 wt.% (*Gerlach*, 1986; *Gerlach et al.*, 2002; *Harris and Anderson*, 1983; *Garcia et al.*, 1989; *Dixon et al.*, 1991; *Anderson and Brown*, 1993; *Wallace and Anderson Jr.*, 1998; *Dixon*

and Clague, 2001; Hauri, 2002; Edmonds *et al.*, 2013; Sides *et al.*, 2014). Similarly, H₂O contents of Kīlauea's parental melts are constrained by melt inclusions and submarine glasses to be approximately 0.7 wt.% or greater (Dixon *et al.*, 1991; Hauri, 2002; Wallace and Anderson Jr., 1998; Clague *et al.*, 1991; Ferguson *et al.*, in preparation). Because Kīlauea's magmas become saturated in CO₂ at depths of about 30-40 km, most of the CO₂ is expected to have exsolved from the magma by the time it enters Kīlauea's summit storage system. Because the bubbles that contain the exsolved CO₂-rich vapor are buoyant, it is thought that most of Kīlauea's CO₂ does not enter the ERZ, but instead escapes to the surface from Kīlauea's summit storage system. Consequently, assuming approximately constant volatile content of Kīlauea's parental melts, the CO₂ emission rate at Kīlauea's summit is considered to be a proxy for deep magma supply rate (Gerlach *et al.*, 2002; Hager *et al.*, 2008).

1.3 Conceptual model

1.3.1 Observational constraints on magma supply

Figure 1.3 displays the estimated supply since 1920 through the magma surge in question. Magma supply rate is based on CO₂ summit emissions (Poland *et al.*, 2012) and GPS measurements of oceanward dilation of the ERZ (Wright and Klein, 2014). This provides a pre-surge flow rate of 0.18 km³ yr⁻¹. CO₂ emissions at the summit suggest a doubling or more from ≈ 8,000 kilotonnes per day to upwards of 20,000 or more, as illustrated in Figure 1.4. Assuming an approximately constant CO₂ content of the parental melt, and likely decoupling of exsolved CO₂ from the

melt beneath Kīlauea's summit, this implies a more than doubling of melt supply.

1.3.2 Model rationale

The purpose of the model is to assess the relationship between magma flow rate, magma pressure, and volatile content of the parental melt, during steady magma ascent to Kīlauea's summit. The model described herein makes judicious simplifications in order to provide a relatively simple and insightful representation of a likely far more complex natural system. For example, it neglects the potential presence of deep storage reservoirs, perhaps near the Moho (*Richards et al.*, 2013; *Pietruszka et al.*, 2015), but for which there is no conclusive evidence. Rather, the intent is an economic representation of essential physical aspects, in order to illuminate the conditions that may contribute to changes in the rate of magma supply, under the constraints of clearly defined assumptions and frugal use of parameters.

It is thought that the deep (lithospheric) magma transport system beneath Kīlauea is some sort of continuously open pathway over decades or longer time periods. One possibility would be some sort of meter-size or larger conduit. This would imply sufficiently low magma ascent velocities and negligibly small viscous pressure losses, and changes in magma pressure with depth would be approximately magma static. Estimates of magma pressure within Kīlauea's shallow storage system indicate at best pressures of about 10 MPa above lithostatic (*Poland et al.*, 2009; *Baker and Amelung*, 2012; *Anderson et al.*, 2015). Consequently, magma pressure at larger depths would be sub-lithostatic by about 100 MPa, neglecting the pres-

ence of olivine crystals suspended in the ascending melt (see Appendix 2.1). A plausible scenario for such a system would probably require thermal equilibrium between magma and wall rock, so that there is a balance between thermal erosion and freezing (*Bruce and Huppert, 1990*). In this case, conduit size would not significantly change in response to changes in magma pressure, except over long time scales due to creep, resulting in a reduction in conduit size until closure or until magma and lithostatic pressure are balanced.

The latter would correspond to a more constricted pathway with the ratio of magma-rock contact area to cross-sectional area sufficiently large to allow for non-negligible viscous pressure losses, such that magma and lithostatic pressure are approximately balanced. One example of such a pathway could be an elastically deformable dike. Neglecting the possibility of viscous relaxation of the surrounding rock or thermal erosion, dike width would then be dependent on the difference between magma and lithostatic pressure, thereby allowing for dynamical feedbacks. This is the model considered herein. Other models or complications are feasible, but are outside the scope of this work.

1.3.3 Essence of the model

The magmatic system at Kīlauea can be conceptually divided into a melting zone, lithospheric pathway, summit storage, and ERZ. Based on this conceptual model, an isothermal model of steady two-phase flow (melt and vapor phase) is considered. Melt first enters the lithospheric pathway with pressure P_b and ascends

through a dike with pressure dependent width. Vapor bubbles grow once the magma pressure becomes sufficiently low to where CO₂-H₂O saturation is reached. The magma pressure at the summit reservoir is P_t . Magma static and frictional pressure losses at a given flow rate Q equal the difference in pressure $P_b - P_t$ (Figure 1.5). Magma exits the lithospheric pathway and may interact with summit reservoir(s), be stored in the ERZ, or erupt at Pu'u Ō'ō.

1.4 Numerical model

1.4.1 Governing equations

Magma ascends from the melt zone beginning at the lithosphere-asthenosphere boundary (a depth of approximately 50 km (*Christensen and Salisbury, 1975; Got et al., 2008; Schmerr, 2012*)), crossing the Moho between 18-19 km depth (*Leahy and Collins, 2010; Rychert et al., 2013*), and finally reaching the deepest identified storage region at around 3.5 - 4 km depth (Figure 1.5; *Baker and Amelung, 2012; Poland et al., 2009, 2014*). I assume magma flow within a dike-like conduit throughout. The dependent variable of interest are magma pressure, P , the average magma ascent velocity, u , and dike width, b . The governing equations for these variables are derived from mass and momentum balance, as well as an equation that relates dike width to magma and lithostatic pressures. In addition, I account for buoyant rise of the magmatic vapor phase (bubbles) using a drift flux formulation, which yields an expression for the volume fraction of vapor, ϕ .

For a dike surrounded by elastically deforming rock, its width is a function of

magma pressure, relative to lithostatic pressure, and the shear modulus of the surrounding rock (*Bokhove et al.*, 2005; *Woods et al.*, 2006; *Costa et al.*, 2007; *Gonnermann and Taisne*, 2015). Thus, dike width, b , is defined as (*Bokhove et al.*, 2005)

$$b = \lambda(P - \kappa P_l). \quad (1.1)$$

Here $\lambda = (1 - \nu)a/G$, ν is Poisson's ratio, a is the length of the dike perpendicular to its width, G is the shear modulus of the country rock, P and P_l are magma static and lithostatic pressures, and κ is a factor that represents the degree of anisotropy of stress orientation present in the lithosphere, (ratio of horizontal to vertical stress). I use $\kappa \approx 1$, to simulate isotropic lithostatic stress. Equation 1.1 holds for dikes with a high aspect ratio $b : a$ (1:100 or 1:1000). At realistic volumetric flow rates Q [m^3/yr], the flow will be laminar. Viscous pressure losses scale inversely with the width of the dike and linearly with magma velocity (*Bokhove et al.*, 2005). Magma density is given as $\rho = (1 - \phi)\rho_m + (\phi)\rho_v$, where ϕ is the volume fraction of exsolved vapor at the given depth, ρ_m is the melt density, and ρ_v is the vapor density at the same depth (*Flowers*, 1979). Magma pressure, P , changes as

$$\frac{dP}{dz} = \rho g + \frac{\gamma \mu u}{b^2}, \quad (1.2)$$

where μ is the melt viscosity and based on the model of *Hui and Zhang* (2007), b is the dike width, u is the mixture velocity, and shape factor $\gamma = 12$ corresponds to flow between two parallel plates.

The value of ϕ is calculated from a drift flux formulation (*Todreas and Kazimi*,

1989), given by

$$\frac{1}{\phi} = C_o \left[1 + \frac{(1-x)\rho_v}{x\rho_m} \right] + \frac{\rho_v V_{vj}}{xM}. \quad (1.3)$$

Here C_o is a constant relating the spatial distribution of the disperse phase ($C_o = 1$ represents an equal distribution of bubbles from the conduit edge to its center (i.e. bubbles don't clump along the wall or center)), x is the flow quality (ratio of vapor mass flux to total (melt + vapor) mass flux), M is mass flux of the mixture, and V_{vj} is the drift velocity of the gas phase relative to the melt phase, given as $V_{vj} = (1 - \phi)^n V_\infty$, $0 < n < 3$. V_∞ is the terminal velocity of a single bubble rising in an infinite liquid (Stoke's velocity). The system contains bubbles < 0.5 cm in diameter, so $n = 3$ and

$$V_\infty = \frac{(\rho_m - \rho_g)d^2}{18\mu}. \quad (1.4)$$

For flows with larger bubbles, corresponding values of n and expressions for V_∞ are defined in Table 11-2 of *Todreas and Kazimi* (1989), reproduced partly in Appendix Table 2.6.

An equation for the change in dike width (Equation 1.6) is obtained from combining the spatial derivative of Equation 1.1 with Equation 1.2. Lastly, I use conservation of mass of melt plus CO_2 and H_2O to derive an equation for the change in mixture (melt plus bubbles) velocity, u . The resultant system of ordinary differential equations is similar to Equations 2.1 *a-b* of *Bokhove et al.* (2005), with the added detail of non-constant magma density due to volatile exsolution and velocity difference between melt and vapor, as well as modified so that a positive increase in

z reflects a deepening from the surface. They are given by

$$\frac{dP}{dz} = -\rho g - \frac{\gamma \mu u}{b^2}, \quad (1.5)$$

$$\frac{db}{dz} = \lambda \frac{dP}{dz} - \lambda \kappa \rho_r g, \quad (1.6)$$

$$\frac{du}{dz} = -\frac{1}{\rho b} \left[u \rho \frac{db}{dz} + u b \frac{d\rho_c}{dz} \right]. \quad (1.7)$$

It is important to note that the density, ρ_c , in the last term of Equation 1.7 is based on a gas fraction, ϕ , of a closed system (equilibrium solubility) degassing path, instead of a gas fraction calculated using drift flux. Thus, ρ_c is an approximation of the mixture density, ρ . Such an approximation is advantageous because ρ_c is only a function of pressure and volatile content, meaning it can be precomputed and then called by the solver, independent of the evolution of ϕ . For justification of this approximation and a numerical expression for $d\rho_c/dz$, the reader is directed to Appendix 2.2. I employ this approximation only when calculating the spatial derivative of density in Equation 1.7.

1.4.2 Initial values

Equations 1.5, 1.6, and 1.7 pose an initial value problem with initial conditions specified at depth $z = z_t = 3.5$, the depth of the deepest summit storage reservoir, and integrated from there to depth $z = z_b$, which represents the depth of the base of the lithosphere (LAB). The initial values thus represent magma pressure, P_t and dike width, b_t . In addition the magma flow rate, Q , is specified. The value of b_t is determined from P_t as

$$b_t = \lambda P_t - \lambda \kappa \cdot P_{l,t}, \quad (1.8)$$

where $P_{l,t}$ is the lithostatic pressure at z_t . Finally, magma velocity is defined as $u_t = Q/\rho ab_t$. Various scenarios can be explored by changing magma pressure P_t , flow rate Q , or both. Additionally, the volatile content dissolved in the primary melt can be varied, which will affect magma density.

1.4.3 Outflow and Storage

Of the three main summit reservoirs, it is thought that magma supplying the ERZ first passes through the deepest reservoir at 3-4 km depth (*Baker and Amelung, 2012; Poland et al., 2014*). Thus, summit inflation or deflation likely represents the balance of inflow from depth and outflow to the ERZ that is modulated by the magma transport capacity of the ERZ. Consequently, when supply from depth increases, magma accumulation in the summit reservoir system invariably also increases reservoir pressure, P_t , thereby causing inflation. Although not modeled, it should be noted that events such as dike propagation, seaward dilation of the ERZ, and increased eruptive activity at Pu‘u ‘Ō‘ō-Kupaianaha are all possible manifestations of the ERZ adjusting to an increase in supply. Such changes may tap stored summit magmas, causing a deflation of the summit.

1.4.4 Volatiles

The primary melt contains dissolved CO_2 and H_2O , which saturate at a pressure some distance above the base of the lithosphere. The mass fraction of exsolved vapor, a CO_2 - H_2O supercritical fluid mixture, is based on the solubility model of

Dixon (1997), assuming equilibrium conditions at any given depth or pressure. Figure 1.6 shows CO₂ and H₂O solubility as a function of pressure, as well as the density of a magma (melt + vapor) under equilibrium, closed-system, static (no flow) conditions. The vapor phase is modeled as a non-ideal supercritical fluid (*Flowers, 1979*)(see Appendix 2.3).

Vapor and melt flow are modeled as decoupled and dependent on bubble size and number density, following a two-phase mixture formulation (e.g., *Todreas and Kazimi, 1989*) where the relative ascent velocity between vapor bubbles and the melt is calculated using a drift-flux formulation where ascent velocity of bubbles will be larger than melt velocity and depends on the bubble size and gas volume fraction. Consequently, volume fraction of gas and, hence, magma density can vary with pressure, flow rate and dike width. Magma density is also affected by pressure and concentration of dissolved volatiles (*Lange, 1994*, see also Appendix 2.4). Although there may be olivine crystallization adding a third phase to the system, it is not considered in this model (Appendix 2.1).

1.4.5 Lithostatic stress

Dike width depends on the difference between magma pressure and lithostatic stress, which is assumed to be non-deviatoric. The latter depends on lithospheric density, as illustrated in Figure 1.6. Below 20 km density is assumed to be ≈ 3200 kg/m³, which represents the lithospheric mantle. The abrupt change in density at a depth of 20 km represents a compositional change to basaltic crust, defining the

Moho. Finally, the gradual decrease in density above 20 km represents layering of intrusive rocks with surface flows as the volcano grew, as well as increasing porosity of rocks that make up the volcanic edifice.

1.5 Results

This section first discusses a non-dimensional analysis of the governing equations, and then an application of the dimensional model to Kīlauea.

1.5.1 Non-dimensional analysis

Full details of the non-dimensionalization are included in Appendix 2.5. In contrast to the dimensional case, a melt of constant density and with no separate vapor phase is considered. Both length scales are normalized by an initial dike width, b_t ; thus, dike width b becomes $\hat{b} = b/b_t$, and depth z is recast as $\hat{z} = z/b_t$. The initial condition is dike width b_t and flow rate Q is specified. The governing equations are integrated from $\hat{z} = 0$ downward. Note that $b_t = \lambda\Delta P_t$, which ties the dike width to the overpressure in the conduit. Thus, the system of equations is given by

$$\frac{d\hat{b}}{d\hat{z}} = - \left[A - B \frac{\hat{u}}{(\hat{b})^2} \right], \quad (1.9)$$

$$\frac{d\hat{u}}{d\hat{z}} = - \frac{\hat{u}}{\hat{b}} \frac{d\hat{b}}{d\hat{z}}, \quad (1.10)$$

where A and B are constants that depend on the boundary conditions b_t and Q , and other parameters.

Solutions for a range of initial conditions are illustrated in Figure 1.7. Dikes width either increases or decreases with depth; however, all dikes eventually reach a depth where width no longer changes, referred to herein as the *decoupling depth* and represents the depth to which pressure changes within the summit reservoir system will affect dike width.

I write an expression for this condition in terms of $\hat{b} = \hat{b}_{eq}$ by solving Equation 1.9 for $d\hat{b}/d\hat{z} = 0$:

$$\begin{aligned} A &= -B \frac{\hat{u}_{eq}}{(\hat{b}_{eq})^2} = -\frac{B}{(\hat{b}_{eq})^3} \\ \hat{b}_{eq} &= \sqrt[3]{-\frac{B}{A}} = \sqrt[3]{-\frac{Q\gamma\mu}{g\Delta\rho a(b_t)^3}}. \end{aligned} \quad (1.11)$$

The depth at which \hat{b}_{eq} is first reached, denoted as \hat{z}_{eq} , is shown in Figure 1.8 as a function of \hat{b}_{eq} . The factor that most significantly impacts \hat{b}_{eq} is b_t . If dimensionalized using values for Kīlauea, and assuming cases where $\hat{z}_{eq} =$ either 1000 or 2000, dike widths of 0.1 to 10 m would yield decoupling depths of 100 m and 20 km, respectively. This implies that a range of surface conditions would only affect dike width down to a maximum depth of ≈ 20 km.

1.5.2 Dimensional model, with application to Kīlauea

First, I apply the model to Kīlauea's activity prior to the surge, and then explore scenarios that would apply during a doubling of the supply rate from depth, including the role of dissolved volatile content in the primary melt.

Reference case

Pre-2003 conditions are defined as an average of $0.18 \text{ km}^3 \text{ yr}^{-1}$ ($\approx 5.7 \text{ m}^3/\text{s}$) of magma arriving from depth that supplies summit chambers, dilation of the ERZ, and the eruption at Pu‘u ‘Ō‘ō (Figure 1.3), corresponding to a summit CO_2 emission rate of 8-10 kilotonnes per day (Figure 1.4). The primary melt contains 0.7 wt% CO_2 and 0.68 wt% H_2O . Using this flow rate, a dike length of 500 m, and an overpressure of 5 MPa (magma pressure of 5 MPa in excess of lithostatic at that depth), the solution yields a dike that narrows with depth (Figure 1.9) for nearly 10 km below the summit chamber and narrows again when crossing the Moho. Gas fraction ϕ remains less than 0.015, and magma velocity is less than 0.18 m/s, slowing where the dike widens. There is a depth at which the dike seems to stabilize in width, similar to what is found in the non-dimensional case. To evaluate the surge condition, I explore changes in pressure and in volatile content in the primary dissolved melt.

Change in bottom pressure

To assess the basal pressure required to sustain a given flow rate, models for a range of flow rates are shown in Figure 1.10. Interestingly, doubling of the flow rate requires less than 0.1 MPa increase in bottom overpressure (magma pressure in excess of lithostatic at that depth). Figure 1.11 shows the corresponding dike width as a function depth. Despite different summit pressures, b_t , dike widths converge to a near constant value with only slight differences in P_b . For most

scenarios, dikes converge above the Moho, but at increases in P_t of > 10 MPa relative to the pre-surge case, the dike converges at or just below the Moho due to the significant change in lithospheric density.

Changes in volatiles

When the volatile content of the melt is changed the pre-surge flow rate yields a different ΔP_b , due to the modified density of the magma. To account for this difference, flow rate is adjusted until the solution yields the same ΔP_b predicted for the reference case. For this constant value of ΔP_b , the effect of changing the CO₂ (and H₂O) content of the parental melt is examined (Figure 1.12). As expected, predicted flow rates increase more when both CO₂ and H₂O are changed, as opposed to CO₂ only. In either case, however, doubling the amount of volatiles produces only a modest increase in magma supply despite presumably doubling summit CO₂ emission rates.

1.6 Conclusion

This study explored fluid-dynamic controls on the supply to Kīlauea volcano by modeling the flow of magma from depth to the surface within a dike with pressure-dependent width. It is found that the elastic response of the wall rock essentially decouples the summit chamber from the pressure state at depth. If an elastically deformable dike is a realistic approximation for Kīlauea, it seems unlikely that changes in summit activity or conditions will affect deep magma supply. Conse-

quently, observed changes in magma supply to Kīlauea would be best explained by small changes in deep magma pressure, perhaps due to transient changes in effective permeability of the melting and/or melt accumulation zone at the base of the lithospheric magma pathway. Last but not least, changes in the volatile content of the melt supplied to Kīlauea is unlikely to significantly affect magma supply rate.

Acknowledgement of support

This material is based upon work supported by the National Science Foundation under grants NSF EAR-1145187 and NSF EAR-1331088. Any opinions, findings, and conclusions or recommendations expressed in this material are those of the author(s) and do not necessarily reflect the views of the National Science Foundation.

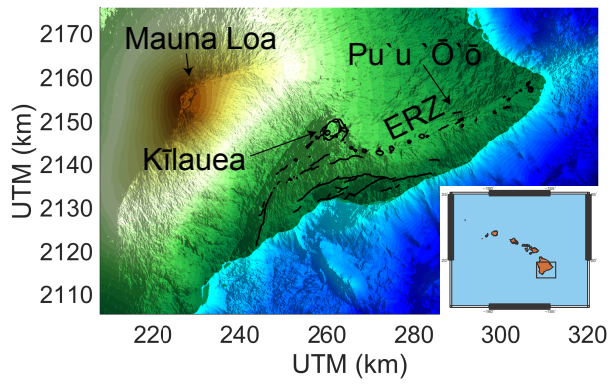


Figure 1.1 : Shaded-relief map showing the southern half of the island of Hawai'i along with notable features of the volcanic system, including the East Rift Zone (ERZ). Inset map was generated using GMT Plotting Tools.

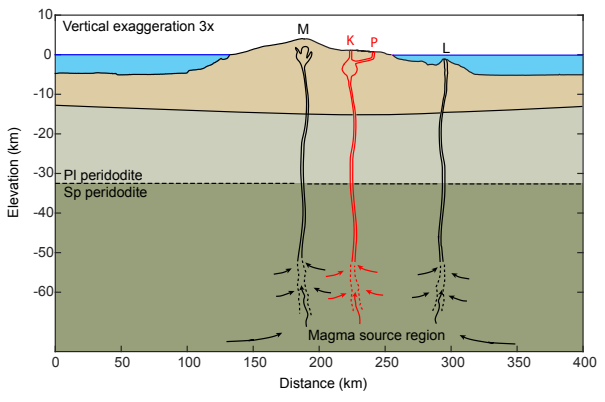


Figure 1.2 : Conceptual model of the magmatic plumbing system beneath Hawai'i, including Kīlauea. The letters **M**, **K**, **P**, and **L**, represent Mauna Loa, Kīlauea, Pu'u Ō'ō, and Loih'i, respectively.

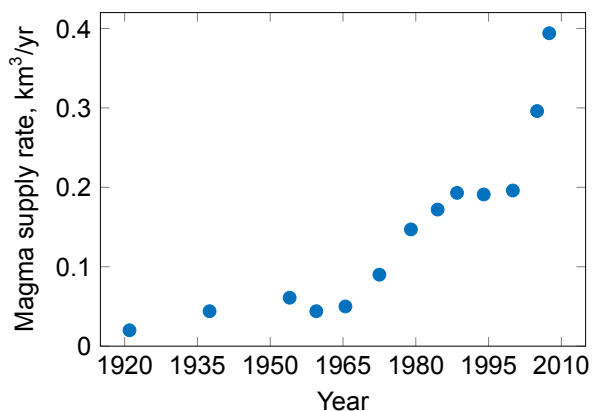


Figure 1.3 : Magma supply rates from *Wright and Klein (2014)*. These rates are estimated by the eruptive and intruded volumes over specific time scales. Supply increased from 1960-1995, but not as dramatically as the 2003-2007 magma surge.

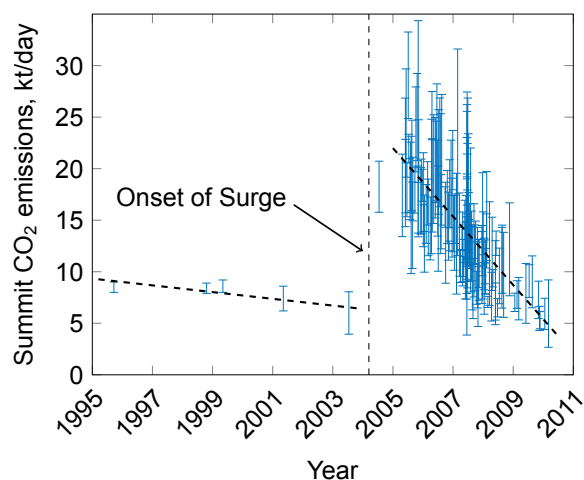


Figure 1.4 : Figure showing the measured CO₂ emissions at Kīlauea's summit (*Poland et al., 2012*). Before the end of 2003, CO₂ emissions remained relatively steady at approximately 8,000 tonnes per day. By 2005, however, emissions increased to nearly 20-30 kilotonnes per day. Emissions began to fall and by 2011 had returned to their pre-surge levels. Black trend lines represent a least squares best fit through the data.

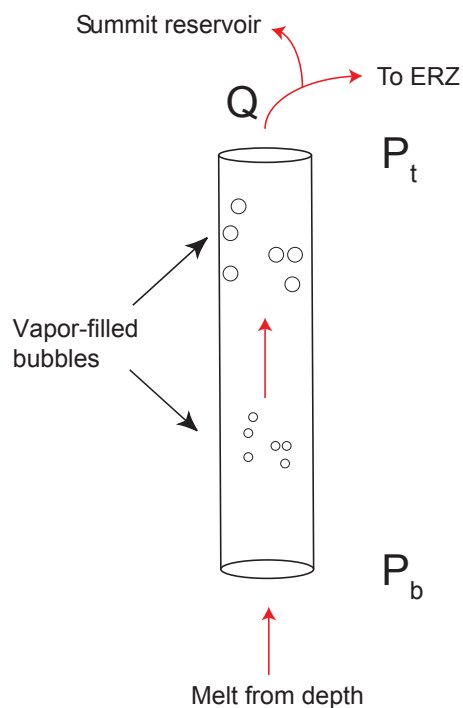


Figure 1.5 : Conceptual model. Melt generated in the asthenospheric melt zone begins to ascend within a dike-shaped conduit, with pressure, P_b . Vapor-filled bubbles form once the ascending melt reaches a pressure where CO_2 saturates. As the magma continues to rise, more CO_2 exsolves and the bubbles grow, becoming more buoyant and rising faster than the host melt. A drift-flux formulation accounts for the differential velocity between the vapor and melt. Finally, magma exits the lithospheric pathway with pressure P_t and flow rate Q , where it may interact with summit reservoir(s) or enter the East Rift Zone (ERZ). The aperture of the dike depends on the overpressure in magma and thus is variable with depth.

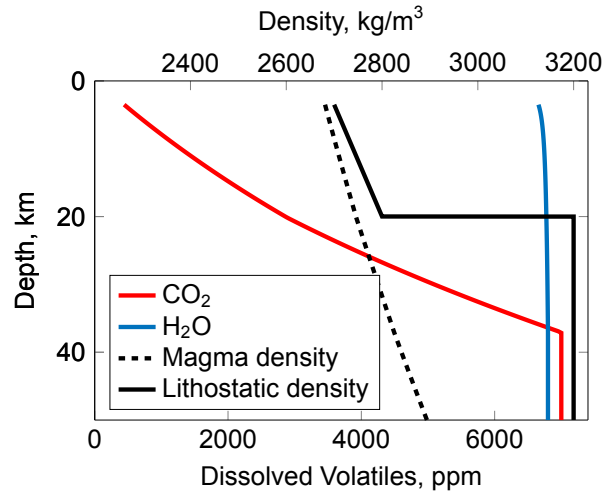


Figure 1.6 : Plot of CO₂-H₂O solubility (*Dixon, 1997*), bulk magma density (*Lange, 1994*) under static closed-system conditions, and lithostatic density as functions of depth. For the depths considered in this model, CO₂ is the dominant component of the vapor phase.

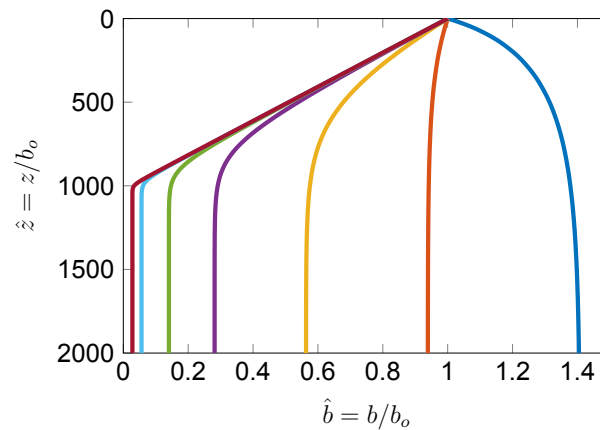


Figure 1.7 : Non-dimensional dike width, $\hat{b} = b/b_t$, as a function of non-dimensional depth, $\hat{z} = z/b_t$, for a range of overpressures in a magma chamber ($\hat{z} = 0$). Shown here is one dike that widens with depth, and several others that narrow with depth. At a unique depth ratio \hat{z} for each set of boundary conditions, dikes no longer change width.

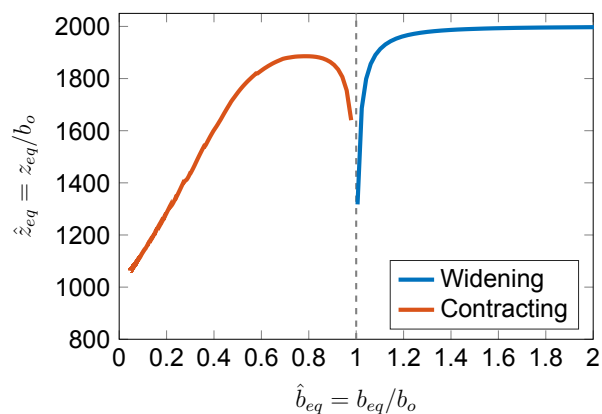


Figure 1.8 : Figure displaying the relationship of equilibrium ($\hat{d}b/d\hat{z} = 0$) values of \hat{b} and its corresponding depth ratio, \hat{z} . Interestingly, two distinct regimes exist: dikes that widen with depth and those that narrow with depth.

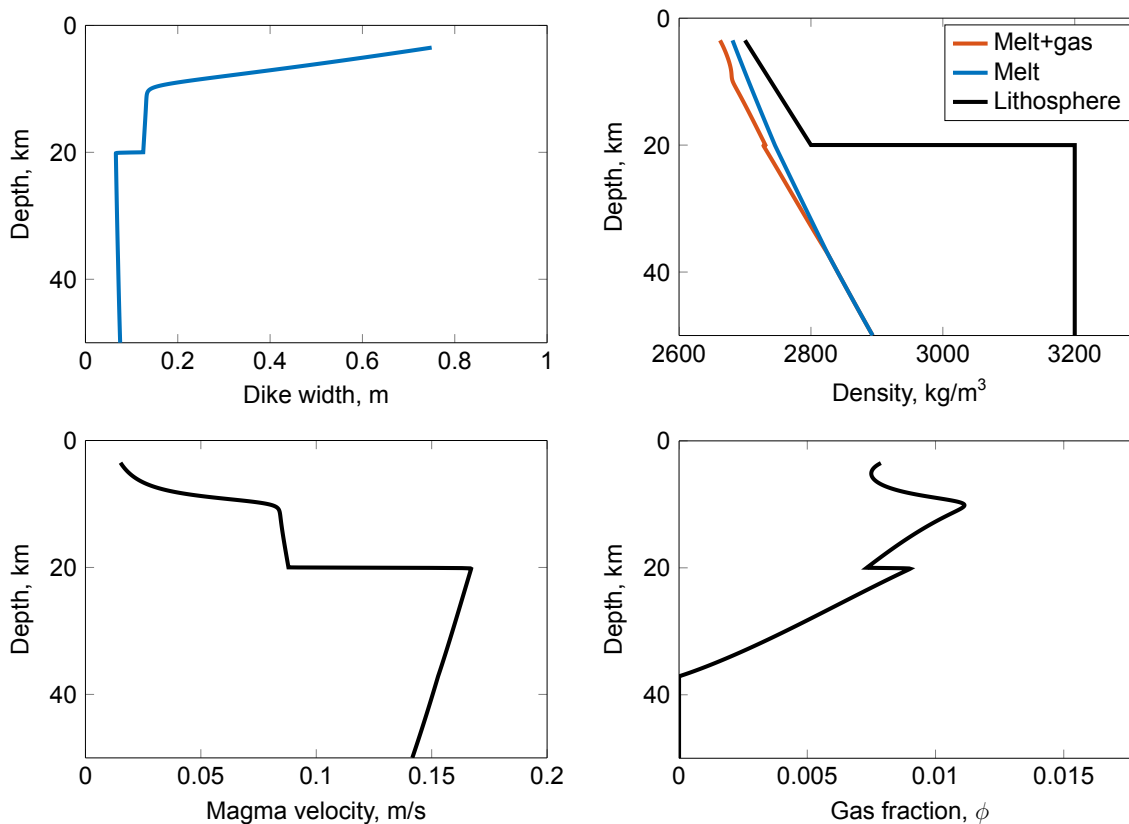


Figure 1.9 : Various parameters of a pre-surge reference case where $Q = 0.18$ km^3/yr and $\Delta P_t = 5$ MPa, and a primary melt containing 0.7 wt% CO_2 and 0.68 wt% H_2O .

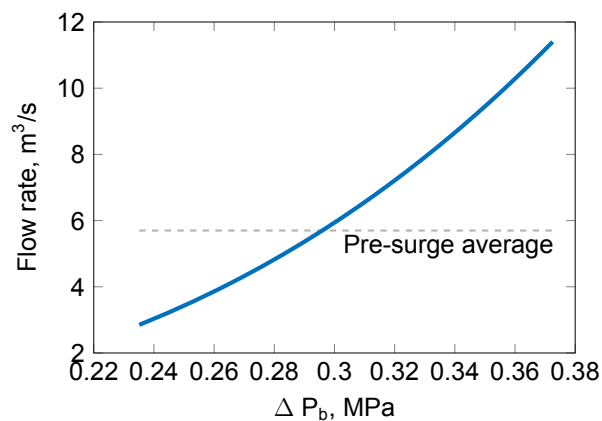


Figure 1.10 : Predicted supply to Kīlauea volcano for a range of overpressures (magma pressure in excess of lithostatic) at the base of the lithosphere (ΔP_b).

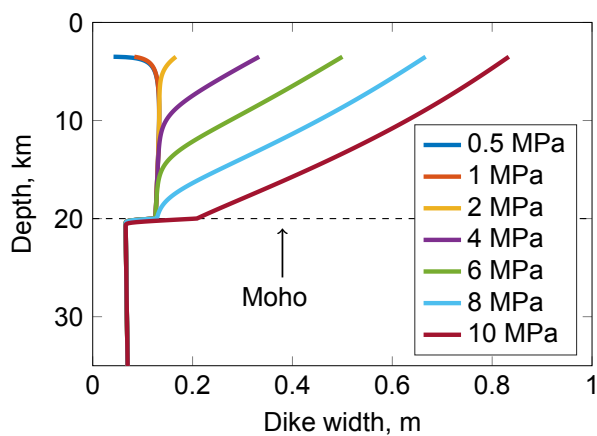


Figure 1.11 : Dike width versus depth for a range of overpressures (magma pressure in excess of lithostatic) at the summit chamber. Below the Moho, all dikes converge to a similar width, regardless of their overpressure in the summit chamber. This *decoupling* of overpressure near the surface and depth suggests that surface conditions have limited effect on supply rate.

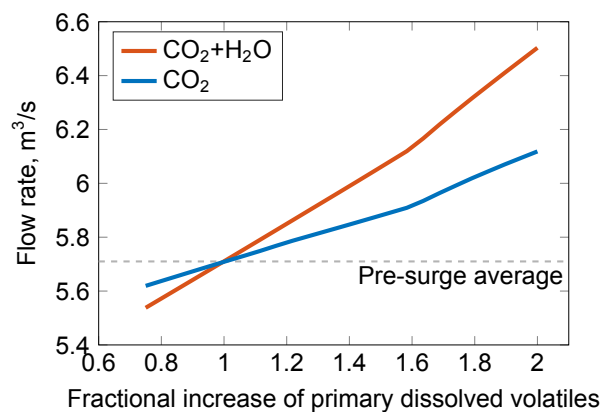


Figure 1.12 : Predicted supply to Kīlauea volcano for melts containing a range of CO₂ and H₂O. A factor of 1 indicates a primary melt composition of 0.7 wt% CO₂ and 0.68 wt% H₂O. Blue curve represents melts that only change in CO₂ whereas the red curve represents melts whose variability is in both volatile species. A change in slope between 1.6 and 1.8 marks the transition from melts that saturate in CO₂ at depths shallower than the inferred lithosphere-asthenosphere boundary (50 km depth) and those that exsolve a vapor phase at pressures higher than those found at 50 km depth.

Table 1.1 : Table listing variables and descriptions used in the model.

Variable	Description
Q	Magma supply rate, km^3/yr
z	Depth, km
P_t	Pressure at the top of the lithospheric pathway
ΔP_t	Magma overpressure at top of lithospheric pathway, ≈ 3.5 km depth
P_b	Pressure at the base of the lithospheric pathway
ΔP_b	Magma overpressure at base of lithospheric pathway
u	Magma velocity
V_{dj}	Relative drift velocity between gas and melt phases
b	Dike width, m
a	Dike length, m
A	Cross-sectional area of conduit
ρ_m	Melt phase density
ρ_g	Gas phase density
ρ	Magma density
ϕ	Gas fraction or porosity
μ	Melt viscosity during ascent (1-10 Pa s)
N_b	Bubble number density
g	Gravity
G	Shear modulus of wall rock

Chapter 2

Appendix

2.1 Olivine crystallization

Olivine that crystallizes during ascent is more dense than the ascending magma. However, their small radius (0.5-2.0 mm (*Clague and Denlinger, 1994; Sides et al., 2014*)) causes them to remain largely entrained and coupled to the magma. Figure 2.3 shows the Stoke's velocity of such olivine crystals. Their settling velocity is between 10^{-3} and 10^{-5} m/s, at least one or two orders of magnitude smaller than the magma ascent velocity (10^{-1} - 10^{-2} m/s). The model predicts a similar magnitude for the vapor phase.

The other effect olivine is on the bulk density of the mixture. Although not equal, the more dense olivine would cancel out any effect of the less dense vapor phase. As noted in Figure 1.12, volatile content has minimal effect on supply rate, and adding more dense olivine to the magma would weaken that effect even further.

In the presence more CO₂ in the primary melt, olivine crystallization may be more favorable. If additional crystals are small, however, they too will remain largely coupled to the melt. The minimal impact of olivine on the model warrants its exclusion.

2.2 Calculating the spatial gradient in mixture density

From mass balance, I derive this equation for the change in mixture velocity:

$$\frac{du}{dz} = -\frac{1}{\rho b} \left[u\rho \frac{db}{dz} + ub \frac{d\rho}{dz} \right]. \quad (2.1)$$

Since mixture density is written as $\rho = \rho_m - \phi\rho_m + \phi\rho_v$, its spatial derivative is written as

$$\frac{d\rho}{dz} = \frac{dP}{dz} \left[(1 - \phi) \frac{d\rho_m}{dP} + \phi \frac{d\rho_v}{dP} \right] + (\rho_v - \rho_m) \frac{d\phi}{dz}. \quad (2.2)$$

Here, ϕ would be calculated using drift flux, accounting for a decoupled vapor phase. This would require a more involved expression for $d\phi/dz$, derived from the drift flux formulation. I choose instead to use a mixture density computed from a gas fraction, ϕ , from a closed system (equilibrium solubility, no flow) degassing path in calculating the second term in Equation 2.1 only. Therefore, closed system mixture density is a function of pressure, denoted $\rho_c(P)$, that can be called to approximate the derivative:

$$\frac{d\rho}{dz} \approx \frac{d\rho_c}{dz} = \left. \frac{d\rho_c}{dP} \right|_{P(z)} \cdot \frac{dP}{dz} \quad (2.3)$$

The magma-static pressure gradient is already calculated, so all that remains is to provide a discretized approximation of the pressure derivative of ρ_c . A centered finite difference formulation is employed to approximate the derivative so that

$$\frac{d\rho_c}{dP}(P_i) \approx \frac{\rho_c(P_i + \Delta P) - \rho_c(P_i - \Delta P)}{2\Delta P}.$$

I compare an *a posteriori* calculation of Equation 2.2 to the approximation used in the model (Equation 2.3), illustrated in Figure 2.2, wherein I conclude that this approximation should not be used in future iterations of the model.

2.3 CO₂-H₂O solubility and gas density

Equilibrium solubility of dissolved CO₂ and H₂O and exsolved gas density are calculated based on *Dixon (1997)*, *Holloway (1977)*, and *Flowers (1979)*. Holding temperature constant, solubility of CO₂ and H₂O in basaltic melt depends on pressure and mole fraction CO₂ (X_{CO_2}) in an exsolved vapor phase. The system is considered both ‘closed’—meaning bubbles remain physically coupled with its parent parcel of melt for the duration of flow from depth to summit—and in equilibrium—meaning the vapor in the bubble remains in equilibrium with the dissolved volatiles via complete diffusion at any given depth. An equation of state (*Holloway, 1977; Flowers, 1979*) provides vapor density, also a function of pressure and X_{CO_2} .

2.4 Melt density and compressibility

Melt compressibility depends on the major oxide composition of the melt, amount of dissolved volatiles, temperature and pressure. Both thermal and pressure expansion as parameterized by *Lange (1994)* for each oxide and volatile components determine the volume of a parcel of melt for a given temperature and pressure. For major oxides, we use a standard Kīlauea melt composition from *Helz (1987)*. Melt volume V (*Lange, 1994*) is given by

$$V_{\text{liq}}(T, P, X_i) = \sum X_i \left[V_{i,T^*} + \frac{dV_i}{dT}(T - T^*) + \frac{dV_i}{dP}(P - P^*) \right], \quad (2.4)$$

where X_i is the mole fraction for each oxide component, P^* is 1 bar, and T^* is 1673 K. This formulation is valid for 0 to 20 kbar and for the temperature of 1370 K. Thermal and pressure expansion of dissolved CO_2 and H_2O is not well constrained, so a constant volume of 24 and 12 cc per mole, respectively, are used (Lange, 1994). Finally, density of the melt phase is

$$\rho_m = \frac{M_{mol}}{V_{liq}} \quad (2.5)$$

where M_{mol} is the molar mass of the melt based on its major oxides and dissolved volatiles given by the solubility calculation.

2.5 Non-dimensional analysis

I start with these equations (2.4a, b from Bokhove *et al.* (2005))

$$\begin{aligned} \frac{d}{dz}(bu) &= 0 \\ 0 &= -\frac{1}{\rho_m \lambda} \frac{db}{dz} + \frac{(\kappa \rho_r - \rho_m)g}{\rho_m} - \frac{\gamma \mu u}{\rho_m b^2} \end{aligned}$$

Removing ρ_m from the second equation yields:

$$\begin{aligned} \frac{d}{dz}(bu) &= 0 \\ 0 &= -\frac{1}{\lambda} \frac{db}{dz} + (\kappa \rho_r - \rho_m)g - \frac{\gamma \mu u}{b^2}. \end{aligned}$$

To perform the nondimensional analysis, I define the following substitutions:

$$\begin{aligned} b_o &= \lambda \Delta P_o, \text{ where } \lambda = \frac{(1-\nu)a}{G} \\ \hat{z} &= \frac{z}{b_o} \\ \hat{b} &= \frac{b}{b_o} \\ \hat{u} &= \frac{uab_o}{Q} \end{aligned}$$

I rewrite the equations in their non-dimensional forms using the previous substitutions.

$$\begin{aligned} \frac{d}{d\hat{z}}(\hat{b}\hat{u}) &= 0 \\ \frac{b_o}{\lambda b_o} \frac{d\hat{b}}{d\hat{z}} &= g\Delta\rho - \frac{Q\gamma\mu}{a(b_o)^3} \frac{\hat{u}}{(\hat{b})^2} \end{aligned}$$

Simplifying,

$$\begin{aligned} \frac{d}{d\hat{z}}(\hat{b}\hat{u}) &= 0 \\ \frac{d\hat{b}}{d\hat{z}} &= \underbrace{\frac{g\Delta\rho\lambda b_o}{b_o}}_A - \underbrace{\frac{Q\gamma\mu\lambda b_o}{a(b_o)^4}}_B \frac{\hat{u}}{(\hat{b})^2} \\ &= \underbrace{g\Delta\rho\lambda}_A - \underbrace{\frac{Q\gamma\mu\lambda}{a(b_o)^3}}_B \frac{\hat{u}}{(\hat{b})^2} \end{aligned}$$

This will be written as a system of ODEs for both cases:

$$\begin{aligned} dy(1) : \frac{d\hat{b}}{d\hat{z}} &= A - B \frac{\hat{u}}{(\hat{b})^2} \\ dy(2) : \frac{d\hat{u}}{d\hat{z}} &= -\frac{\hat{u}}{\hat{b}} \frac{d\hat{b}}{d\hat{z}} \end{aligned}$$

In these equations, $\hat{z} = 0$ represents the deepest location of the dike. Dike width and melt velocity at depth are given as boundary conditions at that depth, and

then the ODEs are integrated *up* to the surface. It is preferable to specify boundary conditions near the surface, which are far better constrained than those at depth, and integrate *down*, requiring a simple sign adjustment. Now, $\hat{z} = 0$ represents the top of the lithospheric pathway, and \hat{z} increases with depth below the volcano.

The new equations are

$$dy(1) : \frac{d\hat{b}}{d\hat{z}} = - \left[A - B \frac{\hat{u}}{(\hat{b})^2} \right], \quad (2.6)$$

$$dy(2) : \frac{d\hat{u}}{d\hat{z}} = - \frac{\hat{u}}{\hat{b}} \frac{d\hat{b}}{d\hat{z}}, \quad (2.7)$$

with boundary conditions $[\hat{b}_o, \hat{u}_o = 1]$.

Decoupling depth

At some depth \hat{z} , dike width no longer changes with depth. This *decoupling depth* indicates the depth at which the pressure boundary condition no longer affect the dike width, and depends primarily on the initial dike width. *Decoupling depth* \hat{z}_{eq} is defined the integral of $d\hat{b}/d\hat{z}$ until it equals $\hat{b}_o - \hat{b}_{eq}$. Since $\hat{b}_o = 1$ and $\hat{z}_o = 0$ by definition, it follows that

$$\begin{aligned} 1 - \hat{b}_{eq} &= \int_0^{\hat{z}_{eq}} \frac{d\hat{b}}{d\hat{z}} d\hat{z} \\ &= \int_0^{\hat{z}_{eq}} -A + B \frac{\hat{u}}{(\hat{b})^2} d\hat{z} \end{aligned} \quad (2.8)$$

This integral does not have a closed form solution. Figure 1.8 illustrates a numerical approximation. I plot the results as \hat{b}_{eq} versus \hat{z}_{eq} , which represent the values of \hat{b} and \hat{z} where $d\hat{b}/d\hat{z} \approx 0$.

When the problem is recast in dimensional form, similar decoupling behavior is observed (see Figure 1.11). It appears that dikes of various starting widths all converge to nearly similar widths at some depth below the surface.

2.6 Sensitivity to N_b

One assumption in the model pertains to bubble size and coalescence. I assume that the bubble number density (number of bubbles per 1 m^3 of melt) remains constant from the moment CO_2 saturates and exsolves a vapor phase forward. Bubbles then increase in radius as CO_2 solubility continues to decrease with shallowing depth. Also, bubbles are not allowed to coalesce as they rise and grow. Since the model does take into account the differential-velocity of the bubbles relative to the melt due to buoyancy, larger bubbles will begin to drift far ahead of the melt, modifying the gas fraction ϕ . Figure 2.1 show these results. Still, this effect doesn't diminish the decoupling behavior observed earlier between surface and depth.

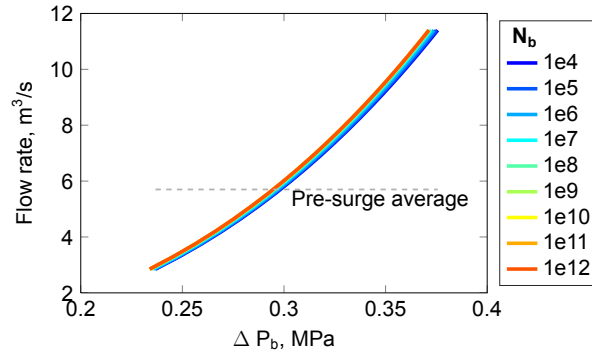


Figure 2.1 : Predicted supply rate to Kīlauea for a range of ΔP_b for a range of plausible bubble number densities. There is no significant difference in flow rate for a given ΔP_b for a range of bubble number densities.

Regime	n	V_∞
Small bubbles ($d < 0.5$ cm)	3	$\frac{g(\rho_l - \rho_v)d^2}{18\mu_l}$
Large bubbles ($d < 2$ cm)	1.5	$1.53 \left[\frac{\sigma g(\rho_l - \rho_v)}{\rho_l^2} \right]^{1/4}$
Churn flow	0	$1.53 \left[\frac{\sigma g(\rho_l - \rho_v)}{\rho_l^2} \right]^{1/4}$

Table 2.1 : Table reproduced in part from Table 11-2 of *Todreas and Kazimi (1989)*, describing values of n and V_∞ .

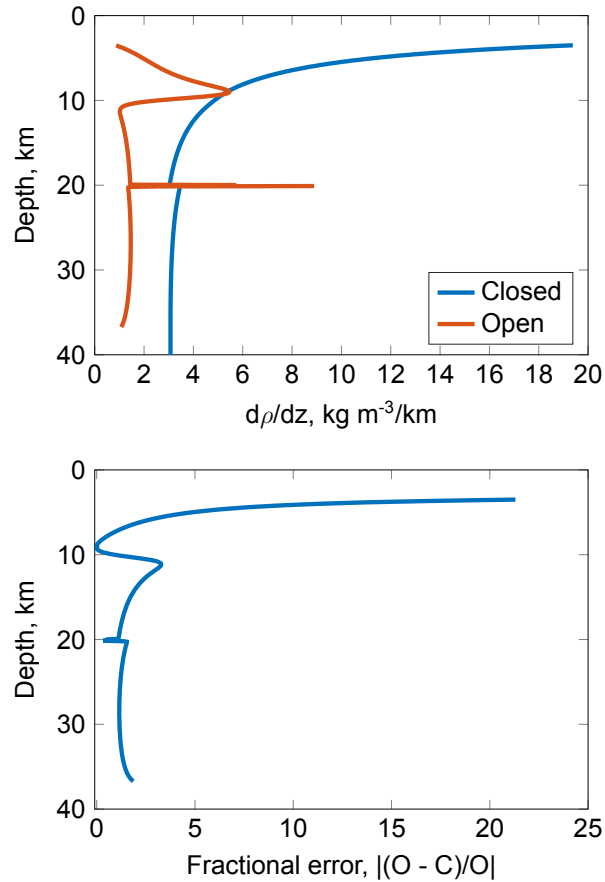


Figure 2.2 : Plots comparing spatial derivatives of mixture density, $d\rho/dz$, as functions of depth. The closed system defines mixture density based on a gas fraction derived from a closed system degassing path, instead of a drift flux value of ϕ . It implies a complete coupling of the vapor phase to the melt. In contrast, the open system bases its mixture density on a gas fraction calculated from drift flux, allowing for a decoupled vapor phase. The open system is calculated *a posteriori* to evaluate the accuracy of using a closed system approximation (Eq. 2.2). The lower plot indicates the fractional error of the approximation, which exceeds 20 near the top of the lithospheric pathway. Due to this error, future iterations will require an implementation of Equation 2.2 in place of the closed system assumption.

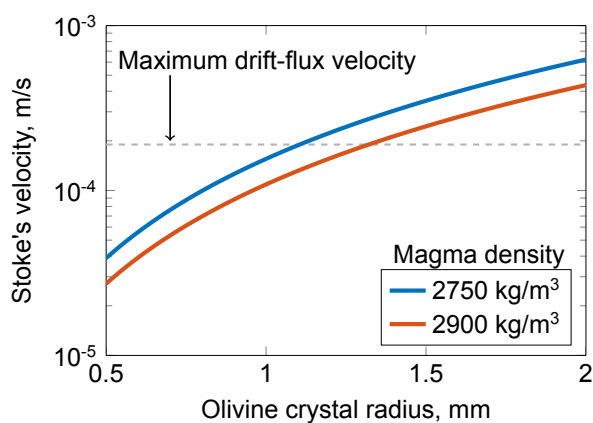


Figure 2.3 : Stoke's velocity versus radius of an olivine crystal suspended in a basaltic melt. Since Stoke's velocity depends on the density of the magma, two curves are plotted that represent an upper and lower bound of magma densities used in the model. Over the size range of olivine crystals reported from other melt inclusion studies (*Clague and Denlinger, 1994; Sides et al., 2014*), velocity varies approximately one order of magnitude, but remains at least an order of magnitude lower than the mixture velocity. For reference, the maximum velocity of the gas phase relative to the melt is plotted.

Bibliography

- Anderson, A. T., and G. G. Brown (1993), CO₂ contents and formation pressures of some Kilauean melt inclusions, *American Mineralogist*, 78(7-8), 794–803.
- Anderson, K. R., M. P. Poland, J. H. Johnson, and A. Miklius (2015), Episodic deflation-inflation events at Kilauea Volcano and implications for the shallow magma system, in *Hawaiian Volcanoes: From source to surface, Geophysical Monograph*, vol. 208, edited by R. Carey, V. Cayol, M. Poland, and D. Weis, pp. 229–250.
- Baker, S., and F. Amelung (2012), Top-down inflation and deflation at the summit of Kilauea Volcano, Hawaii observed with InSAR, *J. Geophys. Res.*, 117, B12,406, doi:10.1029/2011JB009123.
- Bokhove, O., A. W. Woods, and A. de Boer (2005), Magma flow through elastic-walled dikes, *Theor. Comput. Fluid Dyn.*, 19, 261–286, doi:10.1007/s00162-005-0166-4.
- Borgia, A. (1994), Dynamic basis of volcanic spreading, *J. Geophys. Res.*, 99(B9).
- Bruce, P. M., and H. E. Huppert (1990), Solidification and melting along dykes by the laminar flow of basaltic magma, in *Magma Transp. Storage*, edited by M. Ryan, chap. 6, pp. 87–101, John Wiley & Sons Ltd.

- Cao, Q., R. van der Hilst, M. de Hoop, and S.-H. Shim (2011), Seismic imaging of transition zone discontinuities suggests hot mantle west of Hawaii, *Science* (80), 332, 1068–1078.
- Cayol, V., J. H. Dieterich, A. T. Okamura, and A. Miklius (2000), High magma storage rates before the 1983 eruption of Kilauea, Hawaii, *Science*, 288(5475), 2343–2346.
- Cervelli, P., and A. Miklius (2003), The shallow magmatic system of Kilauea Volcano, *US Geol. Surv. Prof. Pap.*, 1676, 149–163.
- Christensen, N. I., and M. H. Salisbury (1975), Structure and constitution of the lower oceanic crust, *Rev. Geophys.*, 13(1), 57, doi:10.1029/RG013i001p00057.
- Clague, D. A., and R. P. Denlinger (1994), Role of olivine cumulates in destabilizing the flanks of Hawaiian volcanoes, *Bulletin of Volcanology*, 56(6-7), 425–434.
- Clague, D. A., W. S. Weber, and J. E. Dixon (1991), Picritic glasses from Hawaii, *Nature*, 353(6344), 553–556.
- Costa, A., O. Melnik, R. S. J. Sparks, and B. Voight (2007), Control of magma flow in dykes on cyclic lava dome extrusion, *Geophys. Res. Lett.*, 34(2), 1–5, doi:10.1029/2006GL027466.
- Delaney, P. T., and D. F. McTigue (1994), Volume of magma accumulation or withdrawal estimated from surface uplift or subsidence, with application to the 1960 collapse of Kilauea Volcano, *Bull. Volcanol.*, 56(6-7), 417–424.

- Delaney, P. T., R. P. Denlinger, M. Lisowski, A. Miklius, P. G. Okubo, A. T. Okamura, and M. K. Sako (1998), Volcanic spreading at Kilauea, 1976-1996, *J. Geophys. Res.*, 103(B8), 18,003–18,023.
- Denlinger, R. A. (1997), A dynamic balance between magma supply and eruption rate at Kilauea volcano, Hawaii, *J. Geophys. Res.*, 102, 18,091–18,100.
- DePaolo, D. J., and E. M. Stolper (1996), Models of Hawaiian volcano growth and plume structure: Implications of results from the Hawaii Scientific Drilling Project, *J. Geophys. Res.*, 101(B5), 11,643–11,654.
- Dixon, J. (1997), Degassing of alkalic basalts, *Am. Mineral.*, 82, 368–378.
- Dixon, J., and D. Clague (2001), Volatiles in basaltic glasses from Loihi Seamount, Hawaii: Evidence for a relatively dry plume component, *J. Petrol.*, 42(3), 627–654, doi:10.1093/petrology/42.3.627.
- Dixon, J. E., D. A. Clague, and E. M. Stolper (1991), Degassing history of water, sulfur, and carbon in submarine lavas from Kilauea Volcano, Hawaii, *J. Geol.*, 99(3), 371–394, doi:10.1086/629501.
- Dvorak, J. J., and D. Dzurisin (1993), Variations in magma supply rate at Kilauea Volcano, Hawaii, *J. Geophys. Res.*, 98, 22,255–22–268.
- Eaton, J., and K. Murata (1960), How volcanoes grow, *Science*, 132(3432), 925–938.
- Edmonds, M., et al. (2013), Magma storage, transport and degassing during the

- 2008-10 summit eruption at Kīlauea Volcano, Hawai‘i, *Geochim. Cosmochim. Acta*, 123, 284–301, doi:10.1016/j.gca.2013.05.038.
- Elias, T., and A. J. Sutton (2007), Sulfur dioxide emission rates from Kīlauea volcano, Hawai‘i, an update: 2002-2006, *U.S. Geol. Surv. Open-File Rept.*, 2007-1114.
- Elias, T., and A. J. Sutton (2012), Sulfur dioxide emission rates from Kīlauea volcano, Hawai‘i, 2007-2010, *U.S. Geol. Surv. Open-File Rept.*, 2012-1107.
- Ferguson, D. J., P. Ruprecht, T. A. Plank, E. H. Hauri, H. B. F., H. M. Gonnermann, and D. A. Swanson (in preparation), Rapid rise of magma modulates explosive basaltic eruptions.
- Flowers, G. (1979), Correction of Holloway’s (1997) adaptation of the modified Redlich-Kwong equation of state for calculation of the fugacities of molecular species in supercritical fluids of geologic interest, *Contrib. to Mineral. Petrol.*, 69, 315–318.
- Frey, F. A., and J. M. Rhodes (1993), Intershield geochemical differences among Hawaiian volcanoes: implications for source compositions, melting process and magma ascent paths, *Phil. Trans. R. Soc. Lond. A*, 342, 121–136.
- Garcia, M. O., D. W. Muenow, K. E. Aggrey, and J. R. O’Neil (1989), Major element, volatile, and stable isotope geochemistry of Hawaiian submarine tholeiitic glasses, *J. Geophys. Res.*, 94(B8), 10,525, doi:10.1029/JB094iB08p10525.
- Garcia, M. O., J. M. Rhodes, F. A. Trusdell, and A. J. Pietruszka (1996), Petrology of

lavas from episodes 2-47 of the Pu‘u ‘Ō‘ō eruption of Kilauea Volcano: III. The Kupaianaha episode (1986-1992), *Bull. Volcanol.*, 58, 359–379.

Garcia, M. O., E. Ito, J. M. Eiler, and A. J. Pietruszka (1998), Crustal contamination of Kilauea Volcano magmas revealed by oxygen isotope analyses of glass and olivine from Pu‘u ‘Ō‘ō eruption lavas, *J. Petrol.*, 39(5), 803–817, doi: 10.1093/petrology/39.5.803.

Garcia, M. O., A. J. Pietruszka, J. M. Rhodes, and K. Swanson (2000), Magmatic processes during the prolonged Pu‘u ‘Ō‘ō eruption of Kilauea Volcano, Hawaii, *J. Petrol.*, 41, 967–990.

Garcia, M. O., A. J. Pietruszka, and J. M. Rhodes (2003), A petrologic perspective of Kilauea Volcano’s summit magma reservoir, *J. Petrol.*, 44, 2313–2339, doi: 10.1093/petrology/egg079.

Gerlach, T. M. (1986), Exsolution of H₂O, CO₂, and S during eruptive episodes at Kilauea Volcano, Hawaii, *J. Geophys. Res.*, 91, 12,177–12,185, doi: 10.1029/JB091iB12p12177.

Gerlach, T. M., K. A. McGee, T. Elias, A. J. Sutton, and M. P. Doukas (2002), Carbon dioxide emission rate of Kilauea Volcano: Implications for primary magma and the summit reservoir, *J. Geophys. Res.*, 107(B9), 2189, doi:10.1029/2001JB000407.

Gonnermann, H. M., and B. Taisne (2015), Magma transport in dikes, *Encyclopedia of volcanoes*, pp. 215–224.

- Got, J. L., V. Monteuiller, J. Monteux, R. Hassani, and P. Okubo (2008), Deformation and rupture of the oceanic crust may control growth of Hawaiian volcanoes., *Nature*, 451, 453–456, doi:10.1038/nature06481.
- Greene, A. R., M. O. Garcia, A. J. Pietruszka, D. Weis, J. P. Marske, M. J. Vollinger, and J. Eiler (2013), Temporal geochemical variations in lavas from Kīlauea's Pu'u 'Ō'ō eruption (1983-2010): Cyclic variations from melting of source heterogeneities, *Geochem. Geophys. Geosys.*, 14, 4849–4873, doi:0.1002/ggge.20285.
- Hager, S. A., T. M. Gerlach, and P. J. Wallace (2008), Summit CO₂ emission rates by the CO₂/SO₂ ratio method at Kilauea Volcano, Hawai'i, during a period of sustained inflation, *J. Volcanol. Geotherm. Res.*, 177, 875–882, doi:10.1016/j.jvolgeores.2008.06.033.
- Harris, D. M., and A. T. Anderson (1983), Concentrations, sources, and losses of H₂O, CO₂, and S in Kilauean basalt, *Geochim. Cosmochim. Acta*, 47(6), 1139–1150, doi:10.1016/0016-7037(83)90244-2.
- Hauri, E. (2002), SIMS analysis of volatiles in silicate glasses, 2: Isotopes and abundances in Hawaiian melt inclusions, *Chem. Geol.*, 183(1-4), 115–141, doi:10.1016/S0009-2541(01)00374-6.
- Head, J. W., and L. Wilson (1992), Magma reservoirs and neutral buoyancy zones on Venus: implications for the formation and evolution of volcanic landforms, *J. Geophys. Res.*, 97, 3877–3903.

- Helz, R. T. (1987), Diverse olivine types in lava of the 1959 eruption of Kilauea Volcano and their bearing on eruption dynamics, in *Volcanism in Hawaii*, USGS Prof. Pap., vol. 1350, edited by R. W. Decker, T. L. Wright, and P. H. Stauffer, pp. 691–722.
- Holloway, J. (1977), Fugacity and activity of molecular species in supercritical fluids, in *Thermodynamics in Geology*, edited by D. Fraser, pp. 161–191, Reidel Publishing Company, Dordrecht Holland, Boston, MA.
- Holtzman, B., and D. Kohlstedt (2007), Stress-driven melt segregation and strain partitioning in partially molten rocks: Effects of stress and strain, *J. Petrol.*, 48(12), 2379–2406, doi:10.1093/petrology/egm065.
- Holtzman, B. K., N. J. Groebner, M. E. Zimmerman, S. B. Ginsberg, and D. L. Kohlstedt (2003), Stress-driven melt segregation in partially molten rocks, *Geochem. Geophys. Geosys.*, 4, 8607.
- Hui, H., and Y. Zhang (2007), Toward a general viscosity equation for natural anhydrous and hydrous silicate melts, *Geochim. Cosmochim. Acta*, 71, 403–416, doi:10.1016/j.gca.2006.09.003.
- Katz, R. F., M. Spiegelman, and B. Holtzman (2006), The dynamics of melt and shear localization in partially molten aggregates., *Nature*, 442(7103), 676–679, doi:10.1038/nature05039.
- Klein, F. W. (1982), Patterns of historical eruptions at Hawaiian volcanoes, *J. Volcanol. Geotherm. Res.*, 12.

- Lange, R. A. (1994), The effect of H₂O, CO₂ and F on the density and viscosity of silicate melts, *Rev. Mineral. Geochem.*, 30.
- Leahy, G. M., and J. A. Collins (2010), Underplating of the Hawaiian Swell: evidence from teleseismic receiver functions, *Geophys. J. Int.*, 183, 313–329, doi: 10.1111/j.1365-246X.2010.04720.x.
- Lister, J. R., and R. C. Kerr (1991), Fluid-mechanical models of crack propagation and their application to magma transport in dykes, *J. Geophys. Res.*, 96(B6), 10,049, doi:10.1029/91JB00600.
- Maaløe, S. (1998), Melt dynamics of a layered mantle plume sources, *Contrib. Mineral. Petrol.*, 133, 83–95.
- Maaløe, S. (1999), Magma accumulation in Hawaiian plume sources, *Am. J. Sci.*, 299, 139–156.
- Maaløe, S. (2003), Melt dynamics of a partially molten mantle with randomly oriented veins, *J. Petrol.*, 44, 1193–1210.
- Maaløe, S. (2005), Extraction of melt from veined mantle source regions during eruptions, *J. Volcanol. Geotherm. Res.*, 147(3-4), 377–390, doi: 10.1016/j.jvolgeores.2005.04.016.
- Maaløe, S., and B. Hansen (1982), Olivine phenocrysts of Hawaiian olivine tholeiite and oceanite, *Contrib. to Mineral. Petrol.*, 81, 203–211.

- Marske, J. P., M. O. Garcie, A. J. Pietruszka, J. M. Rhodes, and M. D. Norman (2008), Geochemical variations during Kīlauea's Pu'u 'Ō'ō eruption reveal a fine-scale mixture of mantle heterogeneities within the Hawaiian plume, *J. Petrol.*, *49*, 1297–1318, doi:doi:10.1093/petrology/egn025.
- McKenzie, D. (1984), The generation and compaction of partially molten rock, *J. Petrol.*, *25*(3), 713–765, doi:10.1093/petrology/25.3.713.
- Miklius, A., and P. Cervelli (2003), Interaction between Kilauea and Mauna Loa, *Nature*, *421*, 229.
- Montgomery-Brown, E. K. (2010), Geodetic evidence for an echelon dike emplacement and concurrent slow slip during the June 2007 intrusion and eruption at Kilauea volcano, Hawaii, *J. Geophys. Res.*, *115*(7), doi:10.1029/2009JB006658.
- Montgomery-Brown, E. K., P. Segall, and A. Miklius (2009), Kilauea slow slip events: Identification, source inversions, and relation to seismicity, *J. Geophys. Res.*, *114*, B00A03, doi:10.1029/2008JB006074.
- Montgomery-Brown, E. K., D. K. Sinnett, K. M. Larson, M. P. Poland, P. Segall, and A. Miklius (2011), Spatiotemporal evolution of dike opening and décollement slip at Kīlauea Volcano, Hawaii, *J. Geophys. Res.*, *116*, doi:10.1029/2010JB007762,.
- Morgan, J. K., G. F. Moore, and D. A. Clague (2003), Slope failure and volcanic spreading along the submarine south flank of Kilauea volcano, Hawaii, *J. Geophys. Res.*, *108*, 2415, doi:10.1029/2003JB002411.

- Morgan, W. (1971), Convection plumes in the lower mantle, *Nature*, 230, 42–43.
- Pietruszka, A. J., K. H. Rubin, and M. O. Garcia (2001), ^{226}Ra - ^{230}Th - ^{238}U disequilibrium of historical Kilauea lavas (1790-1982) and the dynamics of mantle melting within the Hawaiian plume, *Earth Planet. Sci. Lett.*, 186, 15–31.
- Pietruszka, A. J., D. E. Heaton, J. P. Marske, and M. O. Garcia (2015), Two magma bodies beneath the summit of Kilauea Volcano unveiled by isotopically distinct melt deliveries from the mantle, *Earth Planet. Sci. Lett.*, 413, 90–100, doi:10.1016/j.epsl.2014.12.040.
- Poland, M. P., A. Miklius, and T. Orr (2008), New episodes of volcanism at Kilauea Volcano, Hawaii, *EOS*, 89, 37–38.
- Poland, M. P., A. J. Sutton, and T. M. Gerlach (2009), Magma degassing triggered by static decompression at Kilauea Volcano, Hawai'i, *Geophys. Res. Lett.*, 36, L16,306, doi:10.1029/2009GL039214.
- Poland, M. P., A. Miklius, A. J. Sutton, and C. R. Thornber (2012), A mantle-driven surge in magma supply to Kilauea Volcano during 2003-2007, *Nat. Geosci.*, 5, 295–300, doi:10.1038/ngeo1426.
- Poland, M. P., A. Miklius, and E. K. Montgomery-Brown (2014), Magma supply, storage, and transport at shield-stage Hawaiian volcanoes, in *U.S. Geol. Surv. Prof. Pap. 1801*, vol. 2010, edited by M. Poland, T. Takahashi, and C. Landowski, chap. 5, p. 429.

- Reiners, P. W. (2002), Temporal-compositional trends in intraplate basalt eruptions: Implications for mantle heterogeneity and melting processes, *Geochemistry Geophys. Geosystems*, 3(02), doi:10.1029/2001GC000250.
- Ribe, N., and M. Smooke (1987), A stagnation point flow model for melt extraction from a mantle plume, *J. Geophys. Res. Solid*, 92(5), 6437–6443.
- Richards, M., E. Contreras-Reyes, C. Lithgow-Bertelloni, M. Ghiorso, and L. Stixrude (2013), Petrological interpretation of deep crustal intrusive bodies beneath oceanic hotspot provinces, *Geochem. Geophys. Geosys.*, 14, 604–619, doi: 10.1029/2012GC004448.
- Ryan, M. P. (1987), Neutral buoyancy and the mechanical evolution of magmatic systems, *Magmat. Process. Physicochem. Princ.*, 1, 259–287.
- Ryan, M. P. (1993), Neutral buoyancy and the structure of mid-ocean ridge magma reservoirs, *J. Geophys. Res.*, 98(B12), 22,321.
- Rychert, C. A., G. Laske, N. Harmon, and P. M. Shearer (2013), Seismic imaging of melt in a displaced Hawaiian plume, *Nat. Geosci.*, 6(8), 657–660, doi: 10.1038/ngeo1878.
- Schmerr, N. (2012), The Gutenberg discontinuity: Melt at the lithosphere-asthenosphere boundary, *Science*, 335(6075), 1480–1483.
- Scott, D. R., and D. J. Stevenson (1984), Magma solitons, *Geophys. Res. Lett.*, 11(11), 1161–1164, doi:10.1029/GL011i011p01161.

- Scott, D. R., and D. J. Stevenson (1986), Magma ascent by porous flow, *J. Geophys. Res.*, 91(5), 9283–9296, doi:10.1029/JB091iB09p09283.
- Sides, I. R., M. Edmonds, J. Maclennan, D. A. Swanson, and B. F. Houghton (2014), Eruption style at Kilauea Volcano in Hawaii linked to primary melt composition, *Nat. Geosci.*, 7(6), 464–469, doi:10.1038/ngeo2140.
- Sleep, N. H. (1974), Segregation of magma from a mostly crystalline mush, *Geological Society of America Bulletin*, 85(8), 1225–1232.
- Spiegelman, M., and T. Elliott (1993), Consequences of melt transport for uranium series disequilibrium in young lavas, *Earth and Planetary Science Letters*, 118(14), 1 – 20, doi:http://dx.doi.org/10.1016/0012-821X(93)90155-3.
- Sutton, A., T. Elias, T. Gerlach, and J. Stokes (2001), Implications for eruptive processes as indicated by sulfur dioxide emissions from Kilauea volcano, *J. Volcanol. Geotherm. Res.*, 108, 283–302.
- Thornber, C. R., et al. (2003), Kilauea east rift zone magmatism: an Episode 54 perspective, *J. Petrol.*, 44, 1525–1559, doi:10.1093/petrology/egg048.
- Tilling, R. I., and J. J. Dvorak (1993), Anatomy of a basaltic volcano, *Nature*, 363, 125–133, doi:10.1038/363125a0.
- Todreas, N. E., and M. S. Kazimi (1989), *Nuclear Systems I Thermal Hydraulic Fundamentals*, 705 pp., Hemisphere Publishing Corporation.

- Turcotte, D. L., and J. L. Ahern (1978), A porous flow model for magma migration in the asthenosphere, *J. Geophys. Res.*, 83(B2), 767, doi:10.1029/JB083iB02p00767.
- Walker, G. (1992), Coherent intrusion complexes in large basaltic volcanoes: a new structural model, *J. Volcanol. Geotherm. Res.*, 50(1-2), 41–54.
- Wallace, P., and A. Anderson Jr. (1998), Effects of eruption and lava drainback on the H₂O contents of basaltic magmas at Kilauea Volcano, *Bull. Volcanol.*, 59(5), 327–344.
- Wilson, L., and J. W. Head (1988), Nature of local magma storage zones and geometry of conduit systems below basaltic eruption sites: Pu‘u ‘Ō‘ō, Kilauea East Rift, Hawaii, Example, *J. Geophys. Res.*, 93(B12), 14,785–14,792, doi:10.1029/JB093iB12p14785.
- Wolfe, C. J., S. C. Solomon, G. Laske, and J. A. Collins (2009), Mantle shear-wave velocity structure beneath the Hawaiian hot spot, *Science*, 326, 1388–1390.
- Woods, A., O. Bokhove, A. D. Boer, and B. Hill (2006), Compressible magma flow in a two-dimensional elastic-walled dike, *Earth Planet. Sci.*, 246(3-4), 241–250, doi:10.1016/j.epsl.2005.11.065.
- Wright, T., and F. Klein (2006), Deep magma transport at Kilauea volcano, Hawaii, *Lithos*, 87(1-2), 50–79, doi:10.1016/j.lithos.2005.05.004.
- Wright, T. L., and F. W. Klein (2008), Two hundred years of magma transport and storage at Kilauea Volcano, Volcano, Hawai‘i, 1790–2008, in *Dynamics of Crustal*

Magma Transfer, Storage and Differentiation, Geol. Soc. London Spec. Pub., vol. 304, pp. 83–116, doi:10.1144/SP304.5.

Wright, T. L., and F. W. Klein (2014), Dynamics of magma supply to Kilauea volcano, Hawai'i: integrating seismic, geodetic and eruption data, in *Mauna Loa Revealed: Structure, Composition, History, and Hazards, U.S. Geol. Surv. Prof. Pap.*, vol. 1806, p. 240 p., doi:10.3133/pp1806.

Zucca, J. J., D. P. Hill, and R. L. Kovach (1982), Crustal structure of Mauna Loa volcano, Hawaii, from seismic refraction and gravity data, *Bull. Seismol. Soc.*, 72(5), 1535–1550.